Revision 1

Word count:5107

Morphological and chemical characterization of secondary carbonates in the Toki granite, central Japan, and the evolution of fluid chemistry.

Takashi Yuguchi[a,*], Haruka Hatsukawa[a], Satoshi Suzuki[a], Takumi Imura[a], Satoko Motai[a], Kazuo Nakashima[a], and Tadao Nishiyama[b]

[a] Faculty of Science, Yamagata University, 1-4-12 Kojirakawa, Yamagata 990-8560, Japan.

[b] Faculty of Advanced Science and Technology, Kumamoto University, 2-39-1, Kurokami,

* Corresponding author: T. Yuguchi

E-mail address: takashi_yuguchi@sci.kj.yamagata-u.ac.jp

Tel: +81 23 628 4641 / Fax: +81 23 628 4661

ABSTRACT

This study describes the 1) morphological nature of the calcites in the Toki granite, central Japan, 2) difference in chemical compositions in terms of morphological classification, and 3) identification of the stages of calcite formation and the corresponding mass transfer between minerals and fluid owing to hydrothermal alterations and groundwater–rock interactions, which reveals the sequential variations in fluid chemistry during the sub-solidus stage. Calcites in the Toki granite were classified into four types as follows: 1) lenticular calcite in the chloritized biotite, 2) granular calcite in the altered plagioclase, 3) intergranular calcite, and 4) fracture-filling calcite. The lenticular, granular, and intergranular calcites contain greater amounts of iron, manganese, and magnesium than fracture-filling calcites. The lenticular calcite in the chloritized biotite, granular calcite in the altered plagioclase, and intergranular calcite formed due to the precipitation of calcium, iron, manganese, and magnesium released from biotite and plagioclase owing to hydrothermal alterations. The fracture-filling calcites formed at a later stage than the lenticular, granular, and intergranular forms. In the hydrothermal fluid, the concentrations of aluminum, iron, manganese, and magnesium gradually decrease and the concentration of calcium gradually increases as the alteration proceeds. The chemical characteristics of the fluid at the late stage of hydrothermal alteration and those of the subsequent groundwater are consistent with those of fracture-filling calcites, indicating that the fracture-filling calcites precipitated from the fluid at a late stage of hydrothermal alterations and then from the groundwater. Elements released from biotite and plagioclase owing to hydrothermal alterations were incorporated into and fastened to the calcite. Therefore, the calcites

36 influenced the sequential variations in fluid chemistry during the sub-solidus stage.

37

38 Keywords: Carbonate mineral; Calcite; Hydrothermal alteration; Precipitation; Mass
39 transfer; Cathodoluminescence image.

40

This is the peer-reviewed, final accepted version for American Mineralogist, published by the Mineralogical Society of America.
The published version is subject to change. Cite as Authors (Year) Title. American Mineralogist, in press.
DOI: https://doi.org/10.2138/am-2022-8229. http://www.minsocam.org/

41 # INTRODUCTION

42

43 Future forecasting of the geochemical characteristics of a granitic pluton is necessary for
44 safety evaluations of the long-term geological disposal of nuclear waste and underground
45 storage of oil, natural gas, and hydrogen (e.g., Carpenter et al., 2017). For example,
46 whether oxidative fluid (groundwater) will cause the corrosion of artificial metal objects in
47 the facilities can be predicted (Yuguchi et al., 2019). Understanding the long-term history of
48 the chemical characteristics of the hydrothermal fluid and groundwater within a pluton
49 contributes to such forecasts, because the geochemical history of the granite influences the
50 chemical characteristics of the present-day and future groundwater due to water–rock
51 interactions.

52 Carbonate minerals in granitic rock have an important role in evaluating the sequential
53 variations in fluid chemistry. Carbonates are some of the most prevalent secondary minerals
54 in granitic rocks because they readily precipitate from fluids (Munemoto et al., 2015).
55 Calcites of hydrothermal origin in granitic rocks have been recorded to have the chemical
56 characteristics of the original hydrothermal fluid, and those of groundwater origin have
57 been recorded to have the chemical characteristics of groundwater. Many studies have
58 focused on the incorporation of metals and rare earth elements (REEs) in calcium
59 carbonates (e.g., Tanaka et al., 2004; Zhou et al., 2012) because they reflect the
60 precipitation conditions of the source solution (Munemoto et al., 2014). For example,
61 Mizuno and Iwatsuki (2006) revealed the redox conditions of paleo-groundwater based on
62 the uranium and iron contents of fracture-filling calcites. Négrel et al. (2000) demonstrated

63 the similarity in REE patterns between precipitates and groundwater, which was of interest
64 for the precipitation of calcites without ligand exchange of the carbonate aqueous complex
65 between the precipitates and original water. Calcites in granite are known to occur either as
66 a hydrothermal or groundwater origin (Nishimoto et al., 2008; Munemoto et al., 2015). In
67 previous study, there have been few studies relating the chemical composition of carbonates
68 to petrological characteristics, such as morphology and occurrence, except for those on
69 fracture-filling calcites.

70 This study conducted in the Toki granite in Tono district, central Japan focuses on 1) the
71 morphological nature of calcites, 2) the difference in chemical compositions in terms of
72 morphological classifications, and 3) identification of the stages of calcite formation and
73 the corresponding mass transfer between minerals and fluid. The chemistry of the
74 fracture-filling calcites of the Toki granite, which originated from paleo-groundwater, was
75 studied by Iwatsuki et al. (2002) and Munemoto et al. (2014; 2015). Munemoto et al.
76 (2015) revealed the relationship between REEs in deep ground water and those in
77 fracture-filling calcite from the Toki granite, which indicated that the paleo-groundwater
78 was enriched in LREEs and HREEs. The Toki granite consists of hydrothermal-origin
79 calcites, which have a different occurrence than fracture-filling calcites. The hydrothermal
80 alteration in granitic rock is constrained mainly by the dissolution–precipitation processes
81 during the penetration of hydrothermal fluid along microcracks (Nishimoto and Yoshida,
82 2010; Yuguchi et al., 2015). The hydrothermal alteration of the Toki granite progresses
83 through the following successive processes: 1) biotite and hornblende chloritization, 2)
84 plagioclase alteration consisting of albitization, K-feldspathization, illitization, and the

85 formation of fluorite, and 3) the precipitation of calcite minerals (Nishimoto et al., 2008).
86 Calcites in the Toki granite occur in the following four types: lenticular calcites in the
87 chloritized biotite, granular calcites in the altered plagioclase, intergranular calcites, and
88 fracture-filling calcites (see petrography). This study describes the petrography and
89 chemistry of the four types of calcite minerals, which enables us to discuss the nature of
90 calcite precipitation, and the mass transfer between calcites and fluid in a granitic pluton.
91 Furthermore, combining the inferences of this study with those of previous studies on
92 biotite chloritization (Yuguchi et al., 2015), plagioclase alteration (Yuguchi et al., 2019),
93 and hornblende chloritization (Yuguchi et al., 2021) provides a comprehensive
94 characterization of the sequential variation in fluid chemistry during sub-solidus cooling.
95 The Toki granite has two 500 m-long vertical shafts (see Sampling and Analytical
96 Procedures) that enable the extraction of deep drill core samples from within the pluton.
97 These samples have not experienced weathering and are thus suitable for the study of
98 calcites.
99

This is the peer-reviewed, final accepted version for American Mineralogist, published by the Mineralogical Society of America.
The published version is subject to change. Cite as Authors (Year) Title. American Mineralogist, in press.
DOI: https://doi.org/10.2138/am-2022-8229. http://www.minsocam.org/

THE TOKI GRANITE

The Toki granite in the Tono district of central Japan is one of the Late Cretaceous plutonic bodies of the Southwest Japan Arc (Fig. 1A: Ishihara and Chappell, 2007). The Toki granite, is a stock of approximately 14 × 12 km^2 (Ishihara and Suzuki, 1969), which intrudes into the Jurassic sedimentary rocks of the Kamiaso unit in the Mino Terrane (Sano et al., 1992) and into the Late Cretaceous Nohi rhyolite (Sonehara and Harayama, 2007) (Fig. 1B). The Toki granite has a whole-rock Rb–Sr isochron age of 72.3 ± 3.9 Ma (Shibata and Ishihara, 1979), a monazite chemical Th–U–total Pb isochron (CHIME) age of 68.3 ± 1.8 Ma (Suzuki and Adachi, 1998), and a zircon U–Pb isochron age from 74.7 ± 4.2 to 70.4 ± 1.7 Ma (Yuguchi et al., 2016). Based on the phase relationships, Yamasaki and Umeda (2012) estimated that the emplacement depth of granitic magma was approximately 5–7 km below the surface.

The Toki granite, a zoned pluton, has three rock facies grading from muscovite-biotite granite (MBG) at the margin followed by hornblende-biotite granite (HBG) to biotite granite (BG) at the interior (Fig. 1C). The geology and petrography of the Toki granite were described in detail by Yuguchi et al. (2010, 2011A, 2011B). Descriptions and mass transfer of the hydrothermal alteration in the Toki granite have been given by Nishimoto et al. (2008) and Yuguchi et al. (2015; 2019; 2021).

This is the peer-reviewed, final accepted version for American Mineralogist, published by the Mineralogical Society of America.
The published version is subject to change. Cite as Authors (Year) Title. American Mineralogist, in press.
DOI: https://doi.org/10.2138/am-2022-8229. http://www.minsocam.org/

SAMPLING AND ANALYTICAL PROCEDURES

The Mizunami Underground Research Laboratory consists of two vertical shafts (the main and ventilation shafts; Fig. 1D). The main and ventilation shafts are 500 m deep and range from an altitude of 201 masl (meters above sea level; ground level) to −299 masl (shaft bottom; Fig. 1E). The Miocene sedimentary Mizunami Group unconformably overlies the Toki granite, and the unconformity between them is intersected by the shafts at a depth of approximately 170 m.

This study employed borehole 06MI03 (vertical and 336 m long), which was drilled at a depth of 191 m in the ventilation shaft before excavating further below (Fig. 1E). Yuguchi et al. (2015, 2019, 2021) described the petrography and mineral chemistry of biotite and hornblende chloritization, as well as plagioclase alteration in rock samples, at depths from −274 to −314 masl (12 samples spaced 5 m apart) in the ventilation shaft (Fig. 1F). This study employed the same samples as those used by Yuguchi et al. (2015, 2019, 2021) (Table S1). These samples with restricted depth intervals provide rock samples with the same temperature and pressure history during the sub-solidus cooling process of the Toki granite.

Thin sections were prepared to achieve a surface suitable for electron microprobe analysis and cathodoluminescence (CL) imaging by polishing with diamond pastes (particle sizes of 3, 1, and 0.25 μm) to assure the CL-imaging quality (Frelinger et al., 2015). Such careful preparation reduces mineral detachment and adhesive exposure to the observation surface, which allows for high-quality CL imaging. Backscattered electron (BSE) images were generated using a JEOL IT100A scanning electron microscope (SEM) at Yamagata

University, which operates at an accelerating voltage of 15 kV and a beam current of 1.0 nA. The CL patterns reveal the internal structure of carbonates (Bouch, 2006). SEM-CL images were collected using an SEM equipped with a Gatan mini-CL detector (accelerating voltage of 15 kV and beam current of 1.0 nA). The SEM-CL technique enables detailed CL imaging owing to its high resolution and magnification capabilities relative to that of optical-CL images, which greatly improves the ability to observe distinct CL textures (Frelinger et al. 2015). The carbonate excited by a scanned electron beam continues to exhibit luminescence long after the beam has effectively moved on to the next pixel and therefore continues to contribute to the signal received by the detector (Bouch, 2006). This causes "ghosting" or "streaking" across CL images, which prevents the correct analysis of the CL pattern of carbonates. To acquire a CL image without "ghosting" or "streaking," we obtained CL images at a high magnification (more than 2,500× magnification), which result in long pixel dwell times. The long pixel dwell times indicate that the beam moves sufficiently slowly for persistently luminescent materials to stop luminescing before the beam has moved far away from them (Lee et al., 2005). Mineral compositions were analyzed using an electron microprobe analyzer (JEOL JXA-8900) with a wavelength-dispersive X-ray spectrometer at Yamagata University. The analytical conditions maintained for quantitative analysis were an acceleration voltage of 15 kV, a beam current of 15 nA, a beam diameter of 3 μm, and the ZAF data correction method. Carbonate mainly consists of calcite ($CaCO_3$), siderite ($FeCO_3$), magnesite ($MgCO_3$), rhodochrosite ($MnCO_3$), smithsonite ($ZnCO_3$), strontianite ($SrCO_3$), witherite ($BaCO_3$), and cerussite ($RbCO_3$) components (Haldar, 2020). In this study, FeO, MnO, MgO, CaO, SrO,

163 BaO, and PbO were detected during the quantitative analysis of the calcites.

This is the peer-reviewed, final accepted version for American Mineralogist, published by the Mineralogical Society of America.
The published version is subject to change. Cite as Authors (Year) Title. American Mineralogist, in press.
DOI: https://doi.org/10.2138/am-2022-8229. http://www.minsocam.org/

PETROGRAPHY

Sample descriptions

The mineral assemblage of samples No. 1–12 consists of quartz + plagioclase + K-feldspar + biotite ± hornblende, with accessory minerals, such as zircon, apatite, ilmenite, and magnetite, and secondary minerals, such as chlorite, titanite, epidote, allanite, illite, epidote, and calcite. Quartz occurs as equigranular crystals 0.5–25 mm across, with a range of 20.1–32.6 vol% for the mode of each thin section. Plagioclase occurs as subhedral to euhedral crystals 1–20 mm across (mode of 24.8 to 33.8 vol%). K-feldspar is present as subhedral crystals, 1–12 mm across with a perthitic texture (mode of 26.8 to 41.0 vol%). Biotite is variably altered, partially or completely replaced by chlorite. The modes of biotite and chlorite in each thin section represent ranges of 4.6–10.3 vol% and 0.7–3.2 vol%, respectively.

Four occurrences of calcites

Calcites in the Toki granite were classified into four types as follows: 1) lenticular calcite in the chloritized biotite, 2) granular calcite in the altered plagioclase, 3) intergranular calcite, and 4) fracture-filling (vein) calcite (Table S2).

Lenticular calcites in chloritized biotite. Calcites occur in the altered chlorite but do not occur in the non-altered biotite, as shown in Fig. 2. Calcite occurs as lenticular (or columnar) grains along the cleavage of chloritized biotite (less than 35 μm-wide; sample No. 8-2-9 in Fig. 2A). There was a sharp boundary between calcite and chlorite (Fig. 2A-3).

This is the peer-reviewed, final accepted version for American Mineralogist, published by the Mineralogical Society of America.
The published version is subject to change. Cite as Authors (Year) Title. American Mineralogist, in press.
DOI: https://doi.org/10.2138/am-2022-8229. http://www.minsocam.org/

186 Biotite chloritization is associated with the production of secondary minerals, such as
187 titanite, ilmenite, K-feldspar, and fluorite (Yuguchi et al., 2015). The flaky ilmenites are
188 included by calcite and are distributed in contact with the calcites (Fig. 2A-3). The
189 lenticular calcites in the chloritized biotite represent chemical compositions of 93.5–100.0
190 mol% in $CaCO_3$ (calcite component), 0.0–3.8 mol% in $FeCO_3$ (siderite), 0.0–2.4 mol% in
191 $MnCO_3$ (rhodochrosite), 0.0–0.8 mol% in $MgCO_3$ (magnesite), 0.0–0.3 mol% in $SrCO_3$
192 (strontianite), and 0.0–0.1 mol% in $BaCO_3$ (witherite) (N = 94: Table S3).
193
194 **Granular calcites in the altered plagioclase.** Calcites occur within the altered part of
195 plagioclase and do not occur in the non-altered parts (Fig. 3). Plagioclase alteration is
196 associated with albitization, K-feldspathization, illitization, and the formation of fluorite
197 (Yuguchi et al., 2019). The granular calcites are surrounded by alteration-origin albite and
198 K-feldspar (Fig. 3). The granular calcites have various sizes, with those less than 250 μm
199 across (e.g., sample No. 8-1-3 of Fig. 3A-3). There are linear and irregular boundaries
200 between the calcite and surrounding minerals (Fig. 3A-3 and B-3). The granular calcites in
201 the altered plagioclase have chemical compositions of 95.3–100.0 mol% in $CaCO_3$, 0.0–0.8
202 mol% in $FeCO_3$, 0.0–3.9 mol% in $MnCO_3$, 0.0–1.1 mol% in $MgCO_3$, 0.0–0.4 mol% in
203 $SrCO_3$, and 0.0–0.1 mol% in $BaCO_3$ (N = 128: Table S3).
204
205 **Intergranular calcites.** Calcites also occur at grain boundaries among magmatic minerals,
206 for example, the grain boundary among three quartz and one K-feldspar minerals in sample
207 No. 7-2-7 (Fig. 4A) and that among the four plagioclase minerals in sample No. 7-1-3 (Fig.

This is the peer-reviewed, final accepted version for American Mineralogist, published by the Mineralogical Society of America.
The published version is subject to change. Cite as Authors (Year) Title. American Mineralogist, in press.
DOI: https://doi.org/10.2138/am-2022-8229. http://www.minsocam.org/

4B). There are linear and irregular boundaries between the calcite and surrounding minerals (Fig. 4A-2 and B-2). The composition of the intergranular calcite is 95.1–100.0 mol% in $CaCO_3$, 0.0–1.2 mol% in $FeCO_3$, 0.0–3.5 mol% in $MnCO_3$, 0.0–0.3 mol% in $MgCO_3$, 0.0–0.2 mol% in $SrCO_3$, and 0.0–0.1 mol% in $BaCO_3$ (N = 85: Table S3).

Fracture-filling (vein) calcites. They occur in veinlets that are a few micrometers wide (less than 35 μm wide), and there is a sharp boundary between the fracture-filling minerals and the original magmatic minerals (Fig. 5). In the samples, the fracture-filling calcites predominantly occur in quartz and K-feldspar and never in plagioclase and biotite (Fig. 5). The fracture-filling calcites frequently elongate along the microfracture network and grain boundaries (Fig. 5A), and they rarely show a meandering shape, as shown in Fig. 5B. Although lenticular, granular, and intergranular calcites do not show CL patterns reflecting the growth texture, the fracture-filling calcites frequently show stripe patterns, which consist of bright and dark luminescence parts perpendicular to the elongation direction of the fracture (Fig. 5A-3 and A-4). The fracture-filling calcites have a chemical composition of 96.7–100.0 mol% in $CaCO_3$, 0.0–1.7 mol% in $FeCO_3$, 0.0–2.1 mol% in $MnCO_3$, 0.0–0.5 mol% in $MgCO_3$, 0.0–0.1 mol% in $SrCO_3$, and 0.0–0.1 mol% in $BaCO_3$ (N = 266: Table S3).

This is the peer-reviewed, final accepted version for American Mineralogist, published by the Mineralogical Society of America.
The published version is subject to change. Cite as Authors (Year) Title. American Mineralogist, in press.
DOI: https://doi.org/10.2138/am-2022-8229. http://www.minsocam.org/

DISCUSSION

Stages of calcite formation and the corresponding mass transfer

The chemical compositions of the lenticular calcites in the chloritized biotite (Fig. 6A), granular calcites in the altered plagioclase (Fig. 6B), intergranular calcites (Fig. 6C), and fracture-filling calcites (Fig. 6D) are plotted on ternary diagrams with mole percentages of calcite ($CaCO_3$), siderite + rhodochrosite + magnesite ($FeCO_3$+ $MnCO_3$+ $MgCO_3$), and strontianite + witherite ($SrCO_3$+ $BaCO_3$). Fe, Mn, and Mg are richer in the lenticular, granular, and intergranular calcites than in the fracture-filling calcites (Fig. 6).

The alteration processes of biotite chloritization and plagioclase alteration occurred at temperatures of 180–350 °C within the Toki granite (Yuguchi et al., 2015; 2019). Biotite chloritization is characterized by the release of iron, manganese, and magnesium from biotite into fluid (Yuguchi et al., 2015), and the plagioclase alteration is characterized by the release of calcium (anorthite component) from plagioclase into the fluid (Yuguchi et al., 2019). Petrography demonstrates that the chloritized biotite and altered plagioclase include calcites (Figs. 2 and 3). This means that the lenticular calcites in the chloritized biotite and granular calcites in the altered plagioclase were caused by the precipitation of Ca, Fe, Mn, and Mg released from biotite and plagioclase owing to hydrothermal alteration (Fig. 7).

The intergranular calcites include Fe, Mn, and Mg (total of 0–8 mol%), which have similar chemical characteristics to calcites in the chloritized biotite and the altered plagioclase (total of 0–10 mol%); for example, intergranular calcites also formed owing to the precipitation of Ca, Fe, Mn, and Mg released from biotite and plagioclase. Therefore, the lenticular calcites in the chloritized biotite, granular calcites in the altered plagioclase,

and the intergranular calcites were derived from hydrothermal alterations, which occurred at temperatures of 180–350 °C.

Fracture-filling calcites have poor Fe, Mn, and Mg contents (0–3 mol%) relative to the lenticular, granular, and intergranular calcites. Fournier (1990) described that the brittle–plastic transition for silicic rocks can occur at temperatures as high as 370–400 °C in tectonically active regions, such as open fractures in the Toki granite developed at temperatures below 370–400 °C, and the precipitation of Ca along the open fractures could yield fracture-filling calcites. In the hydrothermal fluid of the Toki granite, the concentrations of Al, Fe, Mn, and Mg gradually decreased, and the concentrations of Ca, H, and F gradually increased as the alteration proceeded (Yuguchi et al., 2021). Thus, the hydrothermal fluid that underwent the alteration (i.e., fluid at the late stage of hydrothermal alteration) and the subsequent groundwater exhibits chemical characteristics of abundant Ca and poor Fe, Mn, and Mg contents. The chemical characteristics of the fluid at the late stage of hydrothermal alteration and the subsequent groundwater are consistent with those of fracture-filling calcites, which implies that the fracture-filling calcites precipitated from the fluid during the late stage of hydrothermal alteration and from the subsequent groundwater. Therefore, the fracture-filling calcites occurred at a later stage than the lenticular, granular, and intergranular calcites.

Growth behaviors of fracture-filling calcites deduced from the CL pattern and chemical composition

The growth of calcites occurs perpendicular to the CL band (Bouch, 2006). The

This is the peer-reviewed, final accepted version for American Mineralogist, published by the Mineralogical Society of America.
The published version is subject to change. Cite as Authors (Year) Title. American Mineralogist, in press.
DOI: https://doi.org/10.2138/am-2022-8229. http://www.minsocam.org/

fracture-filling calcites show striped patterns consisting of bright and dark luminescence parts perpendicular to the elongation direction of the fracture (Fig. 5A-3 and A-4). This indicates that the fracture-filling calcites did not grow from the fracture surface (the boundary between the calcite and the host rock) into the interior but that they grew (precipitated) along the elongated direction of the fracture.

Figure 8 shows chemical variations (with mole percentages of $CaCO_3$ and $FeCO_3$+ $MnCO_3$+ $MgCO_3$) along the fracture elongation direction in the calcites (sample No. 2–3). $CaCO_3$ contents increase (Fig. 8B-1) and the sum of $FeCO_3$, $MnCO_3$, and $MgCO_3$ contents decrease (Fig. 8B-2) with distance from the chloritized biotite from 0 to 970 μm. This indicates that 1) the Fe, Mn, and Mg in the fracture-filling calcites were supplied from the chloritized biotite located at a distance of 0 μm, and 2) the fracture-filling calcites precipitated during the hydrothermal alteration stage. Therefore, this chemical gradient along the fracture elongation direction enables us to estimate the source of components that constitute the calcites.

IMPLICATIONS

The methodology and interpretations for providing new insights into the mass transfer owing to hydrothermal alterations and groundwater–rock interactions are described in our serial works (Yuguchi et al., 2015, 2019, 2021 and this study). This study focuses on the petrography and mineral chemistry of calcites in the Toki granite, central Japan. Morphological classifications of calcites and differences in chemical composition lead to differences in the stages of calcite formation and the corresponding mass transfer between minerals and hydrothermal fluid, which has been either overlooked or not fully appreciated in earlier studies. Our serial works reveal the nature of the sequential, long-term variations in fluid chemistry in a granitic pluton across a wide temperature range during sub-solidus cooling, which provides important information for evaluating the evolution of groundwater and water–rock interactions in granite. Methodological combination of 'petrography and mineral chemistry of calcites in this study' and 'developing calcite U-Pb geochronology (e.g., Simpson et al., 2021)' will be able to provide a high-resolution history of the chemical characteristics of the hydrothermal fluid and groundwater within a pluton. Cathodoluminescence and chemical analyses are useful methods for evaluating the growth behavior of fracture-filling calcites.

ACKNOWLEDGEMENTS

We acknowledge the constructive reviews of Dr. Mike Rogerson and Dr. Thomas Mueller (Associated editor), which greatly helped with manuscript revision. This work was financially supported by the Japan Society for the Promotion of Science (JSPS) Grant for Young Scientists [grant number 16H06138], JSPS Grant-in-Aid for Scientific Research (B) [grant number 21H01865], and by a grant from the Ministry of Economy, Trade and Industry (METI), Japan to TY. We would like to thank Editage (www.editage.jp) for English language editing.

REFERENCES CITED

Bouch, J.E. (2006) Development of Capability in the SEM-CL of carbonates. British Geological Survey Internal Report, IR/06/111, pp. 25.

Carpenter, R.H., Reid, J.C., Mysers, C.W. (2017) Underground storage of refrigerated natural gas in granite of the Southeastern U.S. North Carolina Geological Survey, Open-File Report 2017-02, pp. 29.

Frelinger, S.N., Ledvina, M.D., Kyle, J.R., Zhao, D. (2015) Scanning electron microscopy cathodoluminescence of quartz: Principle, techniques and applications in ore geology. Ore Geology Reviews, 65, 840–852.

Fournier, R.O. (1991) The transition from hydrostatic to greater than hydrostatic fluid pressure in presently active continental hydrothermal systems in crystalline rock. Geophysical Research Letters, 18, 955–958.

Haldar, S.K. (2020) Introduction to Mineralogy and Petrology (second edition). Elsevier, pp. 305.

Ishihara, S., Suzuki, Y. (1969) Basement granites of the Toki uranium deposits in Tono region. Reports of the Geological Survey of Japan, 232, 113–127.

Ishihara, S., Chappell, B. (2007) Chemical compositions of the late Cretaceous Ryoke granitoids of the Chubu District, central Japan – Revisited. Bulletin of the Geological Survey of Japan, 58, 323–350.

Itoigawa, J. (1974) Geology of the Mizunami district, central Japan. Bulletin of the Mizunami Fossil Museum, 1, 9–42 (in Japanese).

Itoigawa, J. (1980) Geology of the Mizunami district, central Japan. Monograph of the

333 Mizunami Fossil Museum, 1, 1–50 (in Japanese).

334 Iwatsuki, T., Satake, H., Metcalfe, R., Yoshida, H., Hama, K. (2002) Isotopic and
335 morphological features of granitic calcite from granitic rocks of the Tono area, Japan: a
336 promising palaeohydrogeological. Applied Geochemistry, 17, 1241–1257.

337 Lee, M.R., Martin, R.W., Trager-Cowan, C., Edwards, P.R. (2005) Imaging of
338 cathodoluminescence zoning in calcite by scanning electron microscopy and
339 hyperspectral mapping. Journal of Sedimentary Research, 75, 313–322.

340 Mizuno, T., Iwatsuki, T. (2006) Long-term stability of geochemical environment at deep
341 underground –Case study of minor elements in carbonate minerals–. Chikyukagaku
342 (Geochemisty), 40, 33–45 (in Japanese with English abstract).

343 Munemoto, T., Fukushi, K., Kanzaki, Y., Murakami, T. (2014) Redistribution of Pb during
344 transformation of monohydrocalcite to aragonite. Chemical Geology, 387, 133–143.

345 Munemoto, T., Ohmori, K., Iwatsuki, T. (2015) Rare earth elements (REE) in deep
346 groundwater from granite and fracture-filling calcite in the Tono area, central Japan:
347 Prediction of REE fractionation in paleo- to present-day groundwater. Chemical Geology,
348 417, 58–67.

349 Négrel, P., Guerrot, C., Cocherie, A., Azaroual, M., Brach, M., Fouillac, C. (2000) Rare
350 earth elements, neodymium and strontium isotopic systematics in mineral waters:
351 evidence from the Massif Central, France. Applied Geochemistry, 15, 1345–1367.

352 Nishimoto, S., Ukai, E., Amano, K., Yoshida, H. (2008) Alteration process in deep granitic
353 rock - an example of Toki granite, central Japan. Journal of the Japan Society of
354 Engineering Geology, 49, 94–104 (in Japanese with English abstract).

355 Nishimoto, S., Yoshida, H. (2010) Hydrothermal alteration of deep fractured granite:
356 Effects of dissolution and precipitation. Lithos, 115, 153–162.
357 Sano, H., Yamagata, T., Horibo, K. (1992) Tectonostratigraphy of Mino terrane: Jurassic
358 accretionary complex of southwest Japan. Palaeogeography, Palaeoclimatology,
359 Palaeoecology, 96, 41–57.
360 Shibata, K., Ishihara, S. (1979) Rb-Sr whole-rock and K-Ar mineral ages of granitic rocks
361 in Japan. Geochemical Journal, 13, 113–119.
362 Simpson, A., Glorie, S., Morley, C.K., Roberts, N.M.W., Gillespie, J., Lee, J.K. (2021)
363 In-situ calcite U-Pb geochronology of hydrothermal veins in Thailand: New constraints
364 on Indosinian and Cenozoic deformation. Journal of Asian Earth Sciences, 206, 104649.
365 Sonehara, T., Harayama, S. (2007) Petrology of the Nohi Rhyolite and its related
366 granitoids: a Late Cretaceous large silicic igneous field in central Japan. Journal of
367 Volcanology and Geothermal Research, 167, 57–80.
368 Suzuki, K., Adachi, M. (1998) Denudation history of the high T/P Ryoke metamorphic belt,
369 southwest Japan: constraints from CHIME monazite ages of gneisses and granitoids.
370 Journal of Metamorphic Geology, 16, 27–37.
371 Tanaka, K., Ohta, A., Kawabe, I. (2004) Experimental REE partitioning between calcite
372 and aqueous solution at 25 °C and 1 atm: constrains on the incorporation of seawater
373 REE into seamount-type limestone. Geochemical Journal, 38, 19–32.
374 Todo Collaborative Research Group (1999) Fault bounded inland basin of multiple blocks:
375 an example from the sedimentary basin of the Tokai Group around Tajimi City in Gifu
376 Prefecture, central Japan. Earth Science, 53, 291–306.

377 Yamasaki, S., Umeda, K. (2012) Cooling history of the Cretaceous Toki granite in the
378 eastern Sanyo Belt, Central Japan. Japanese Magazine of Mineralogical and Petrological
379 Sciences, 41, 39–46 (in Japanese with English abstract).
380 Yuguchi, T., Tsuruta, T., Nishiyama, T. (2010) Zoning of rock facies and chemical
381 composition in the Toki granitic body, Central Japan. Japanese Magazine of
382 Mineralogical and Petrological Sciences, 39, 50–70 (in Japanese with English abstract).
383 Yuguchi, T., Tsuruta, T., Nishiyama, T. (2011A) Three-dimensional cooling pattern of a
384 granitic pluton I: The study of exsolution sub-solidus reactions in the Toki granite,
385 Central Japan. Journal of Mineralogical and Petrological Sciences, 106, 61–78.
386 Yuguchi, T., Tsuruta, T., Nishiyama, T. (2011B) Three-dimensional cooling pattern of a
387 granitic pluton II: The study of deuteric sub-solidus reactions in the Toki granite,
388 Central Japan. Journal of Mineralogical and Petrological Sciences, 106, 130–141.
389 Yuguchi, T., Sasao, E., Ishibashi, M., Nishiyama, T. (2015) Hydrothermal chloritization
390 process from biotite in the Toki granite, Central Japan: Temporal variation of chemical
391 characteristics in hydrothermal fluid associated with the chloritization. American
392 Mineralogist, 100, 1134–1152.
393 Yuguchi, T., Iwano, H., Kato, T., Sakata, S., Hattori, K., Hirata, T., Sueoka, S., Danhara,
394 T., Ishibashi, M., Sasao, E., Nishiyama, T. (2016) Zircon growth in a granitic pluton
395 with specific mechanisms, crystallization temperatures and U-Pb ages: Implication to
396 the ‘spatiotemporal’ formation process of the Toki granite, central Japan. Journal of
397 Mineralogical and Petrological Sciences, 111, 9–34.
398 Yuguchi, T., Shoubuzawa, K., Ogita, Y., Yagi, K., Ishibashi, M., Sasao, E., Nishiyama, T.

399 (2019) Role of micropores, mass transfer, and reaction rate in the hydrothermal
400 alteration process of plagioclase in a granitic pluton. American Mineralogist, 104, 536–
401 556.
402 Yuguchi, T., Matsuki, T., Izumino, Y., Sasao, E., Nishiyama, T. (2021) Mass transfer
403 associated with chloritization in the hydrothermal alteration process of granitic pluton.
404 American Mineralogist, in press.
405 Zhou, H., Greig, A., Tang, J., You, C-F., Yuan, D., Tong, X., Huang, Y. (2012) Rare earth
406 element patterns in a Chinese stalagmite controlled by sources and scavenging from
407 karst groundwater. Geochimica et Cosmochimica Acta, 83, 1–18.
408

409 **Figure captions**

410

411 **Figure 1.** The Toki granite and Mizunami Underground Research Laboratory. (A)
412 Location map of the Toki granite (TKG) in central Japan. (B) Geologic map of the Toki
413 granite after Itoigawa (1980), showing the Mizunami Underground Research Laboratory
414 and the borehole sites. Topographic contours are based on Geographical Survey Institute
415 1:25,000 topographic maps, titled "Mitake," "Takenami," "Toki," and "Mizunami." The
416 Toki granite is overlain unconformably by the Miocene Mizunami Group and the
417 Mio-Pleistocene Tokai Group (Itoigawa, 1974; 1980; Todo Collaborative Research
418 Group, 1999). (C) Rock facies cross-section of the Toki granite along the line from X to
419 X' on the geologic map (Fig. 1B) showing three lithofacies (Yuguchi et al. 2010). MBG:
420 muscovite-biotite granite, HBG: hornblende-biotite granite, and BG: biotite granite. (D)
421 Location of the shafts and boreholes in the Mizunami Underground Research Laboratory.
422 (E) Schematic overview of the shafts in the Mizunami Underground Research Laboratory
423 showing the sample locations in this study. The samples were collected from borehole
424 06MI03, at altitudes ranging from −274 masl (meters above sea level) to −314 masl in
425 the HBG of the Toki granite.

426

427 **Figure 2.** Polarization microscope (POM) and backscattered electron (BSE) images of
428 the lenticular calcites in the chloritized biotite (A: sample No. 8-2-9, B: sample No.
429 8-2-5). Numbers in the calcites (A-3 and B-3) correspond to the chemical analysis points
430 listed in Table S3. Cal: calcite, Chl: chlorite, Qtz: quartz, Pl: plagioclase, and Il: ilmenite.

Figure 3. Polarization microscope (POM) and backscattered electron (BSE) images of the granular calcites in the altered plagioclase (A: sample No. 8-1-3, B: sample No. 8-1-7). Numbers in the calcites (A-3 and B-3) correspond to the chemical analysis points listed in Table S3. Cal: calcite, Chl: chlorite and Pl: plagioclase.

Figure 4. Polarization microscope (POM) and backscattered electron (BSE) images of the intergranular calcites (A: sample No. 7-2-7, B: sample No. 7-1-3). Numbers in the calcites (A-2 and B-2) correspond to the chemical analysis points listed in Table S3. Cal: calcite, Qtz: quartz, Pl: plagioclase, and Kfs: K-feldspar.

Figure 5. Polarization microscope (POM), backscattered electron (BSE), and cathodoluminescence (CL) images of the fracture-filling (vein) calcites (A: sample No. 12-2-6, B: sample No. 4-1, and C: sample No. 7-2-4). Numbers in the calcite (A-3) correspond to the chemical analysis points listed in Table S3. Cal: calcite, Bt: biotite, Qtz: quartz, Pl: plagioclase, and Kfs: K-feldspar.

Figure 6. Chemical compositions of lenticular calcites in the chloritized biotite (N = 94), granular calcites in the altered plagioclase (N = 128), intergranular calcites (N = 85), and fracture-filling calcites (N = 266) plotted on ternary diagrams with mole percentages of calcite ($CaCO_3$), siderite + magnesite + rhodochrosite ($FeCO_3$+ $MnCO_3$+ $MgCO_3$), and strontianite + witherite ($SrCO_3$+ $BaCO_3$).

453

454 **Figure 7.** Schematic figure showing the mass transfer of chemical components through
455 hydrothermal fluids during the precipitation of the calcites. Pl: plagioclase and Qtz:
456 quartz.

457

458 **Figure 8.** Chemical variations (with mole percentages of calcite ($CaCO_3$) and siderite +
459 magnesite + rhodochrosite ($FeCO_3$+ $MnCO_3$+ $MgCO_3$)) along the fracture elongation
460 direction in the fracture-filling calcite (sample No. 2-3). (A) Scanning line from 0 to 970
461 μm in the BSE images. (B) Compositional profiles of $CaCO_3$ (mol%: B-1) and $FeCO_3$+
462 $MnCO_3$+ $MgCO_3$ (mol%: B-2). Cal: calcite, Bt: biotite, Qtz: quartz, Pl: plagioclase, and
463 Kfs: K-feldspar.

This is the peer-reviewed, final accepted version for American Mineralogist, published by the Mineralogical Society of America.
The published version is subject to change. Cite as Authors (Year) Title. American Mineralogist, in press.
DOI: https://doi.org/10.2138/am-2022-8229. http://www.minsocam.org/

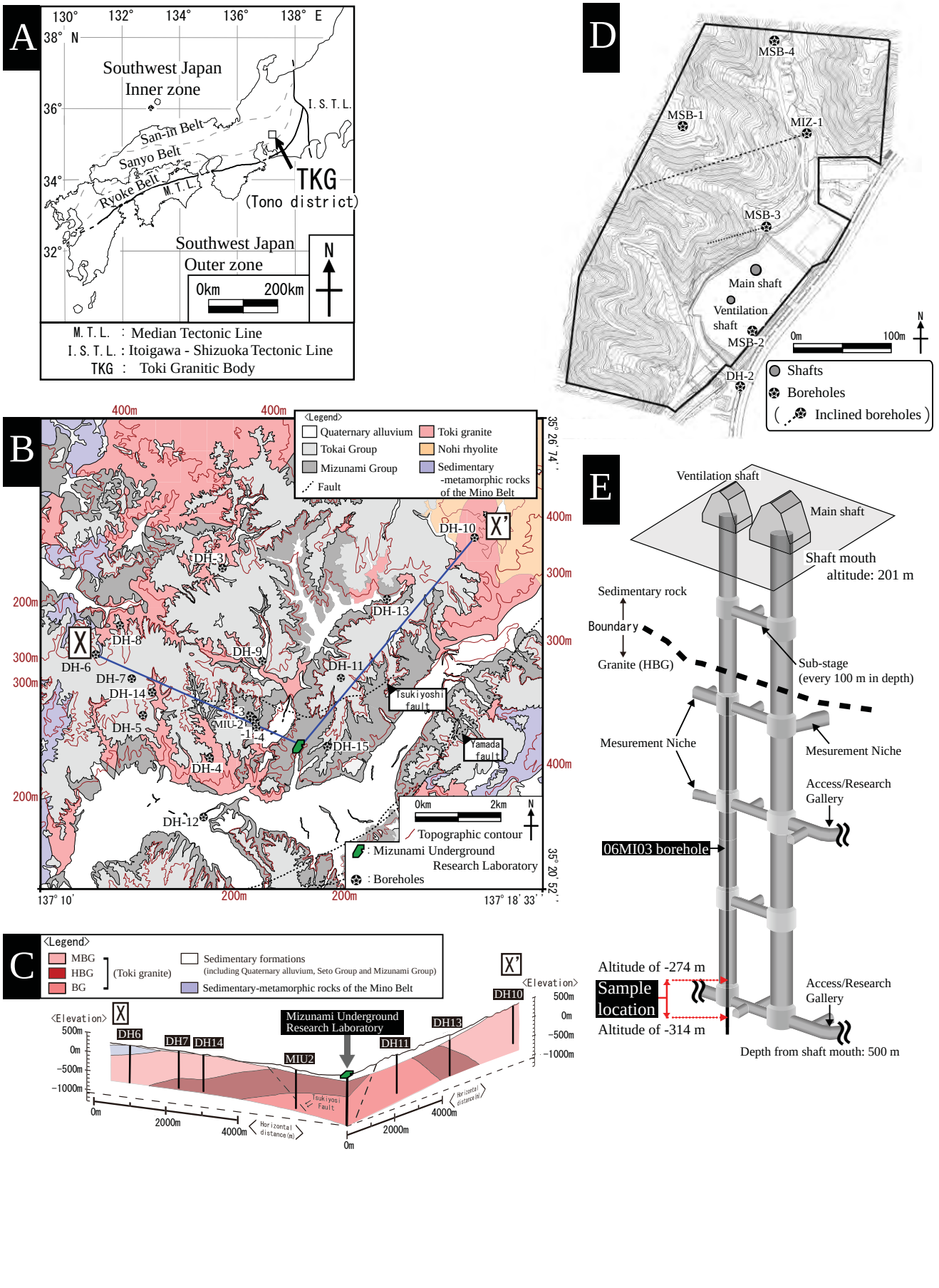

Yuguchi et al. Fig. 1

This is the peer-reviewed, final accepted version for American Mineralogist, published by the Mineralogical Society of America.
The published version is subject to change. Cite as Authors (Year) Title. American Mineralogist, in press.
DOI: https://doi.org/10.2138/am-2022-8229. http://www.minsocam.org/

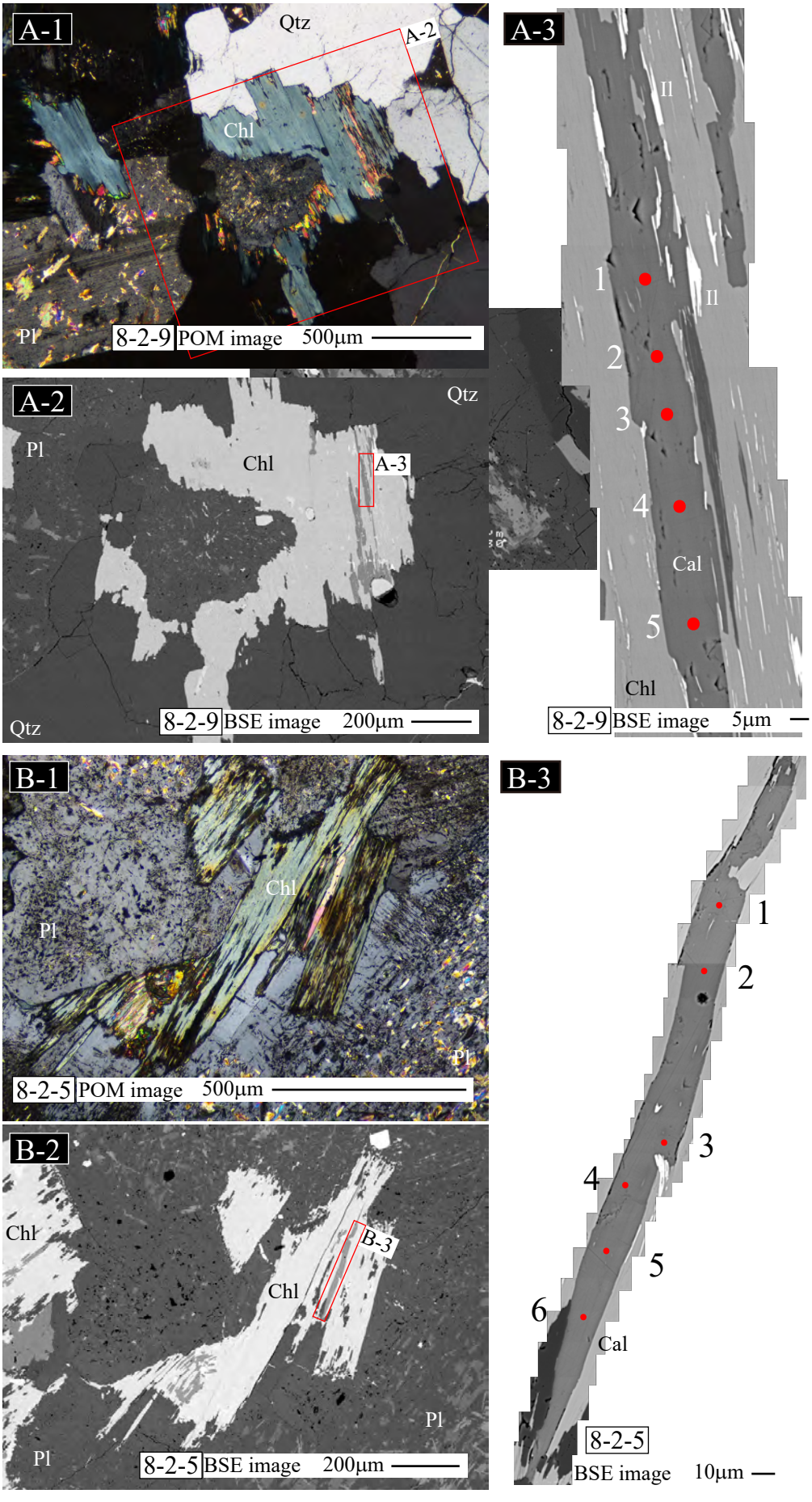

Yuguchi et al. Fig. 2

This is the peer-reviewed, final accepted version for American Mineralogist, published by the Mineralogical Society of America.
The published version is subject to change. Cite as Authors (Year) Title. American Mineralogist, in press.
DOI: https://doi.org/10.2138/am-2022-8229. http://www.minsocam.org/

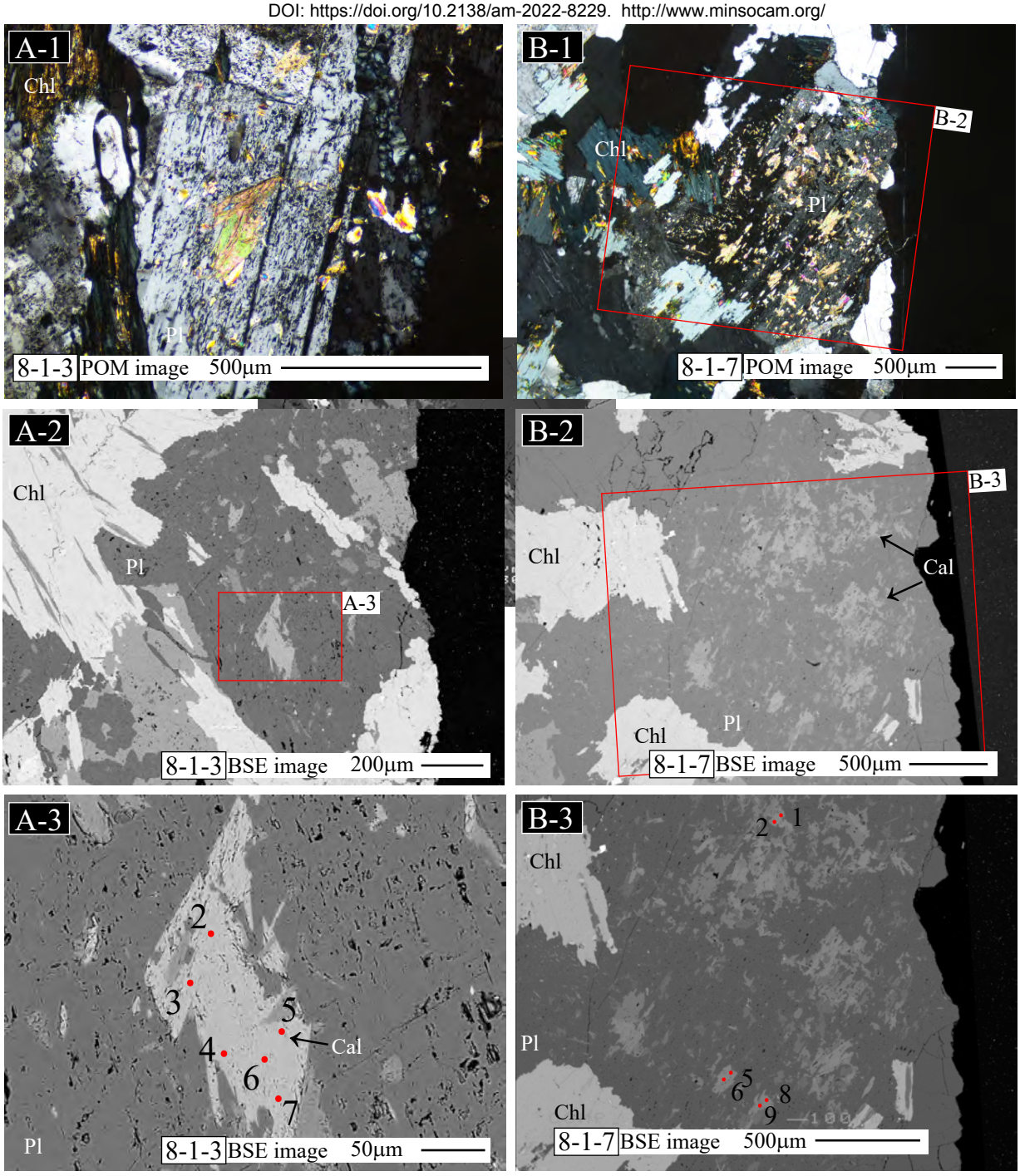

Yuguchi et al. Fig. 3

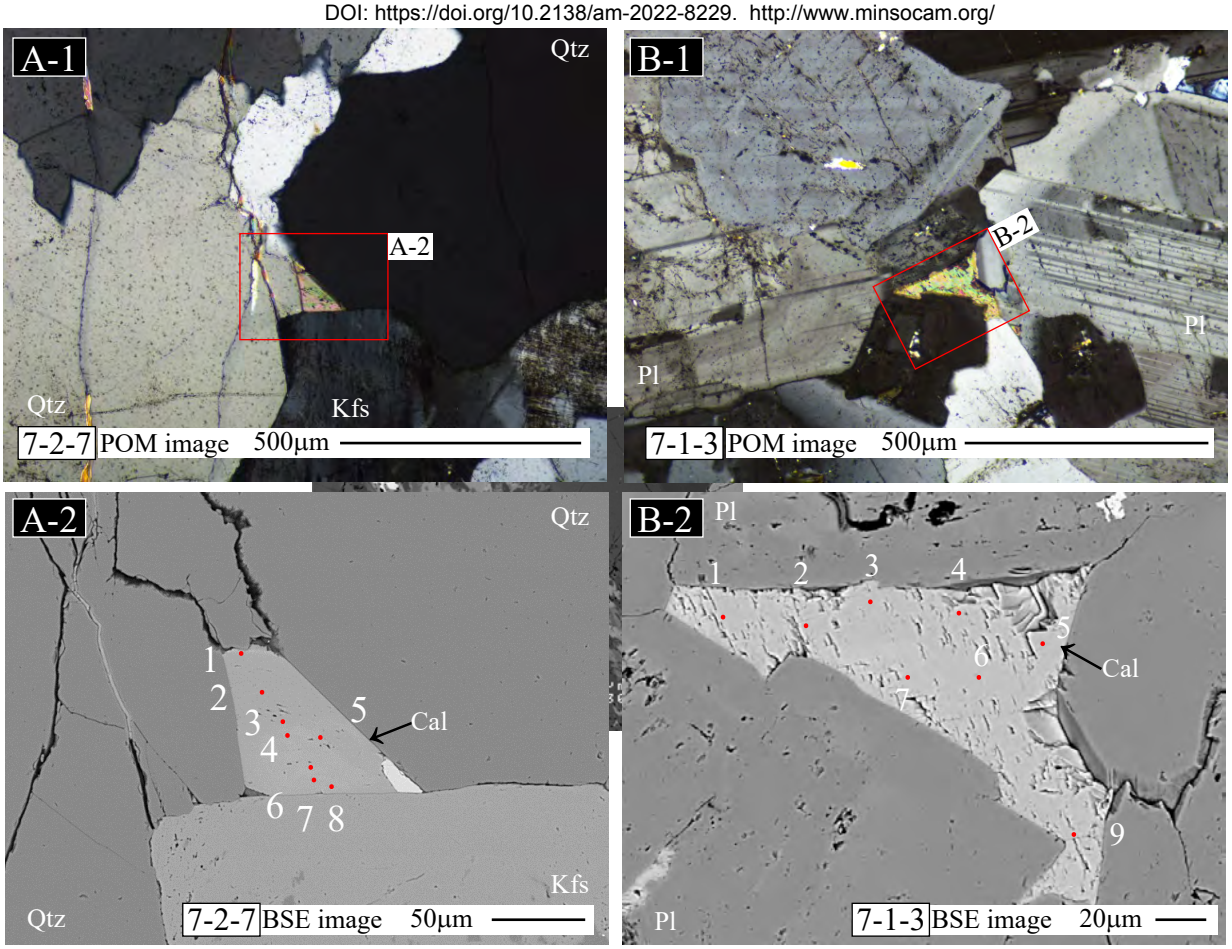

Yuguchi et al. Fig. 4

This is the peer-reviewed, final accepted version for American Mineralogist, published by the Mineralogical Society of America.
The published version is subject to change. Cite as Authors (Year) Title. American Mineralogist, in press.
DOI: https://doi.org/10.2138/am-2022-8229. http://www.minsocam.org/

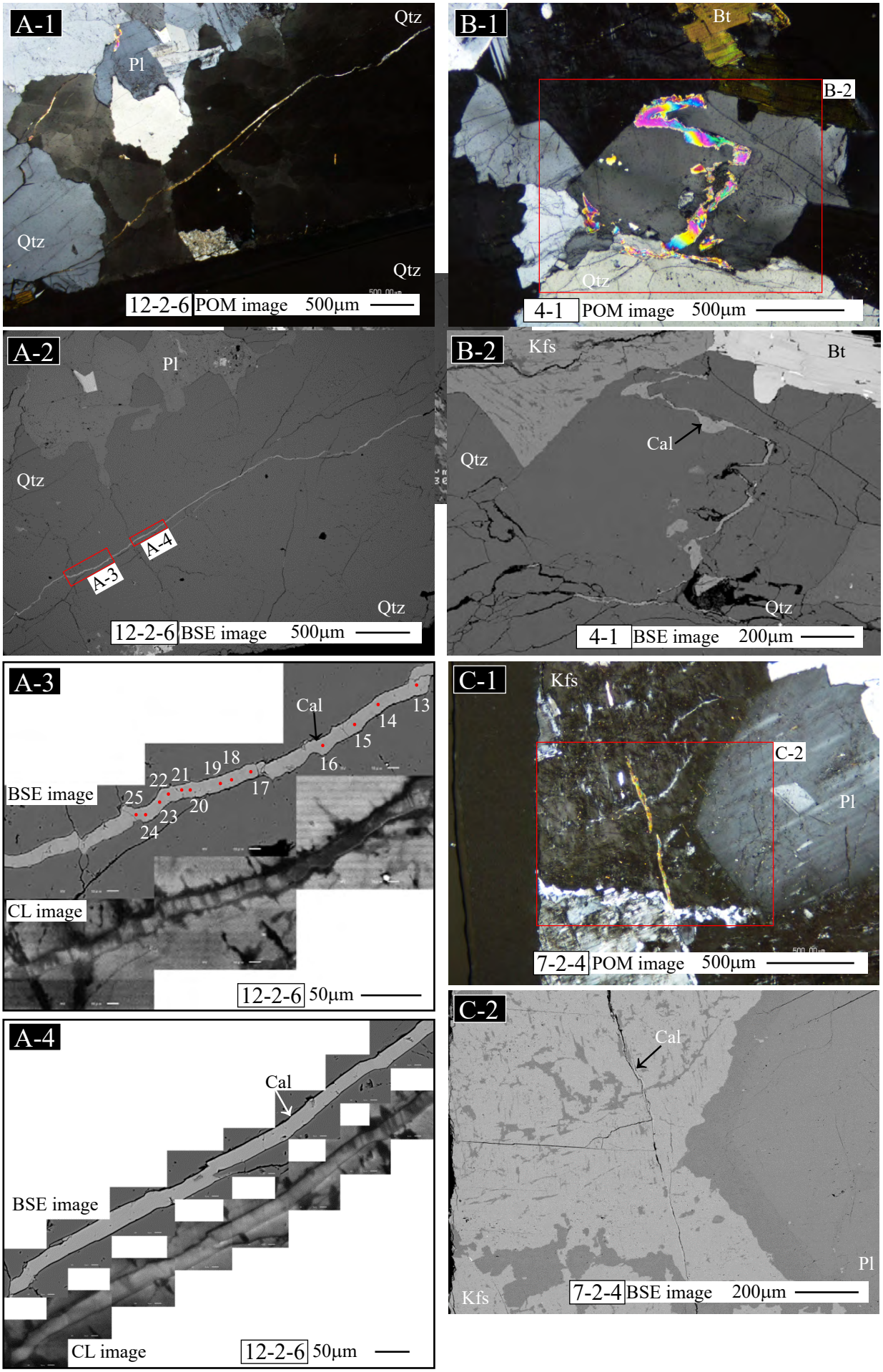

Yuguchi et al. Fig. 5

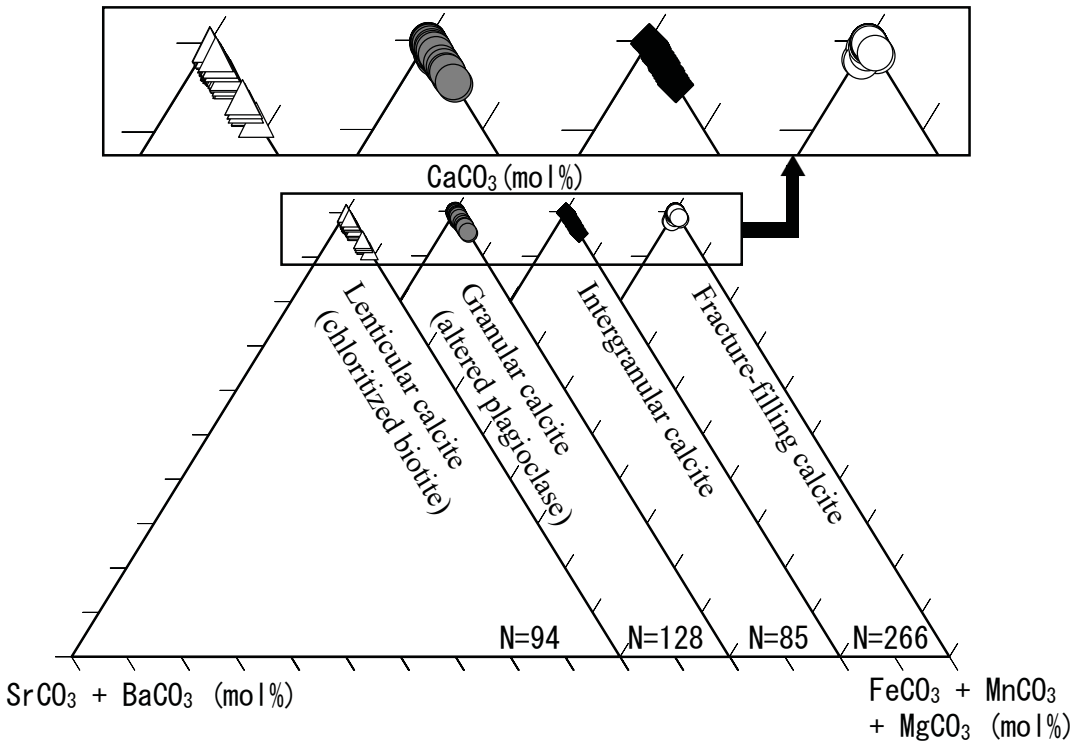

Yuguchi et al. Fig. 6

This is the peer-reviewed, final accepted version for American Mineralogist, published by the Mineralogical Society of America.
The published version is subject to change. Cite as Authors (Year) Title. American Mineralogist, in press.
DOI: https://doi.org/10.2138/am-2022-8229. http://www.minsocam.org/

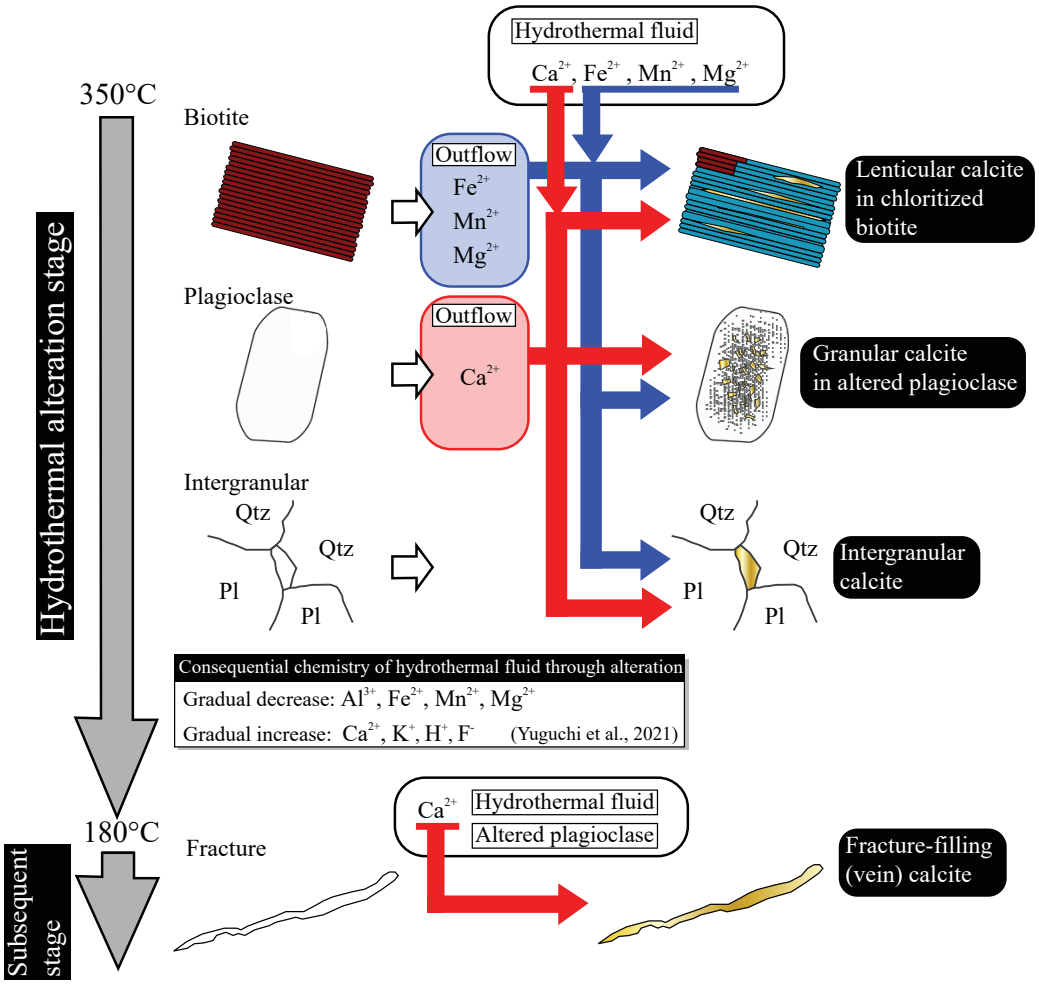

Yuguchi et al. Fig. 7

This is the peer-reviewed, final accepted version for American Mineralogist, published by the Mineralogical Society of America.
The published version is subject to change. Cite as Authors (Year) Title. American Mineralogist, in press.
DOI: https://doi.org/10.2138/am-2022-8229. http://www.minsocam.org/

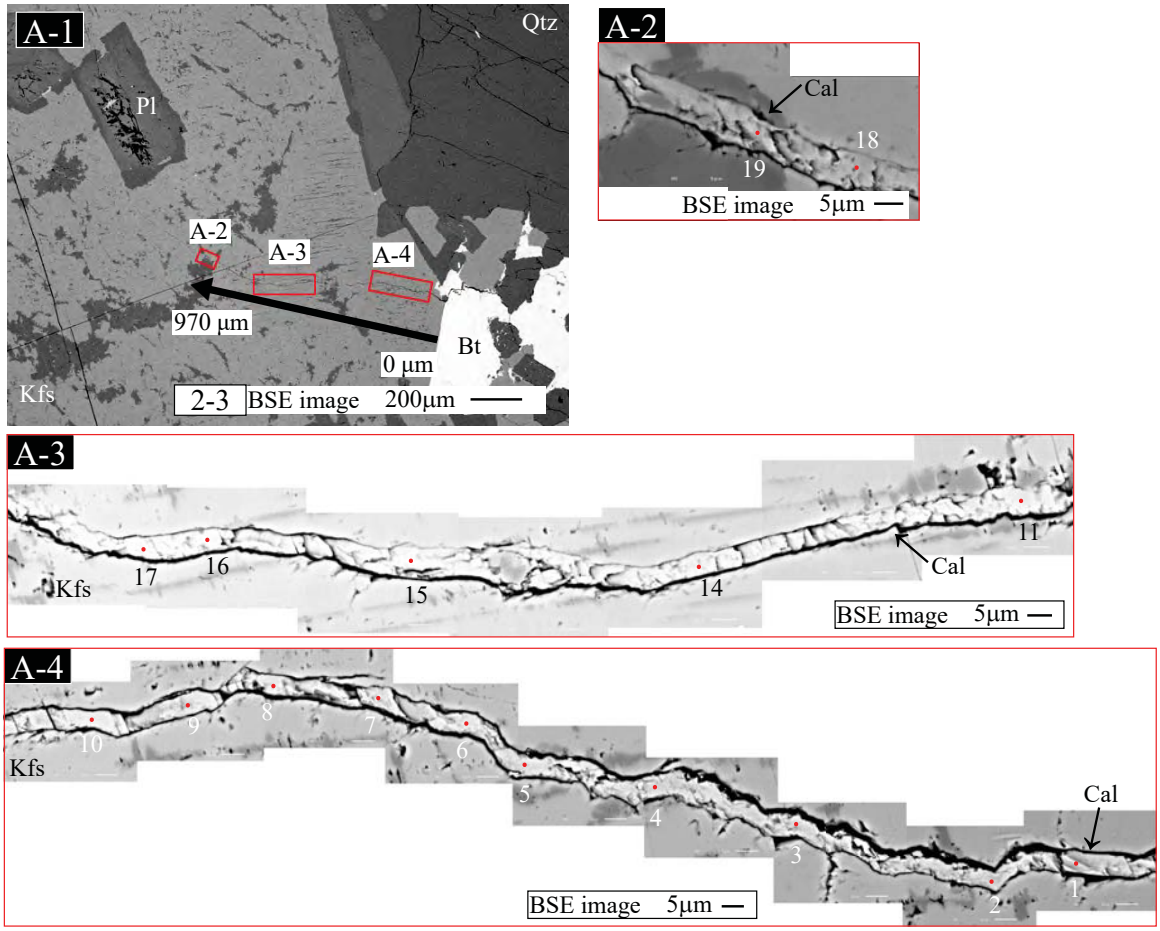

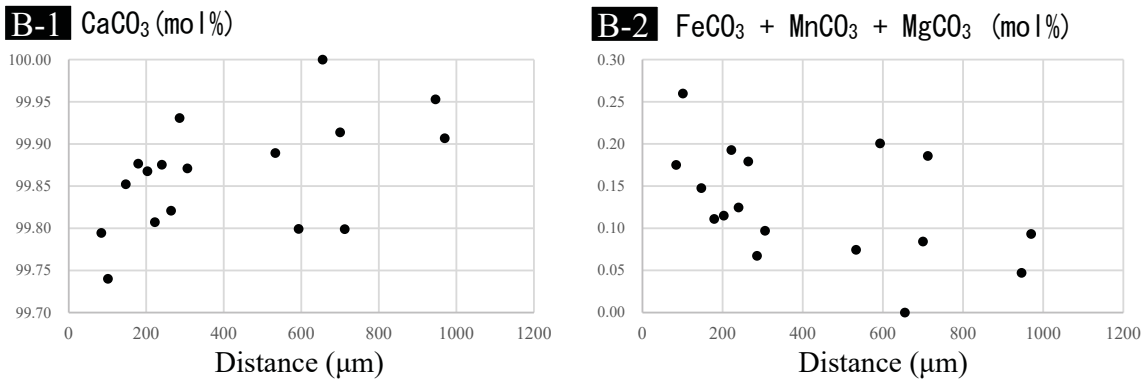

Yuguchi et al. Fig. 8